DFT-BASED FREQUENCY OFFSET ESTIMATORS FOR 16-APSK

Bryan Redd, Jamison Ebert, Autumn Twitchell
Department of Electrical and Computer Engineering
Brigham Young University
Provo, UT, 84606
bryan.d.redd@gmail.com, jamison.ebert@byu.edu, atwitch23@gmail.com

Faculty Advisor:
Michael Rice

ABSTRACT

In this paper, we analyze several DFT-based frequency offset estimators for use with the 16-APSK digital modulation scheme. Even a small frequency offset between radio transmitters and receivers can cause phase information to be lost, so a system to align the phases is required to reliably demodulate PSK signals. These estimators have been adapted for 16-APSK from methods originally intended for use with QPSK and CPM. These methods consist of a coarse search and a fine search with an optional dichotomous search to improve accuracy. We analyze the estimator error variance and bit error rate associated with several methods of frequency estimation. These estimators exhibit small estimate error and variance and can provide bit error rates close to the ideal AWGN BER.

INTRODUCTION

The frequency offset estimator approximates the frequency offset between transmitter and receiver carrier frequencies. When information is encoded in the phase of the transmitted signal, such frequency discrepancies between two carriers will cause the system to fall out of sync and result in a large bit error rate (BER). Therefore, reliable digital communication systems require highly accurate and precise methods of frequency estimation.

The methods used in this paper include methods developed for QPSK and CPM adapted for 16-APSK from [1, 2, 3]. These frequency offset estimation simulations consist of several steps outlined in Figure 1. First, an additive white Gaussian noise (AWGN) channel is simulated by selecting random 16-APSK symbols, modulating those random symbols with a constant frequency offset, adding noise, and then demodulating. After timing synchronization, the matched filter outputs are used for frequency estimation as shown in Figure 2.

The frequency offset must be properly estimated and removed from the received, demodulated

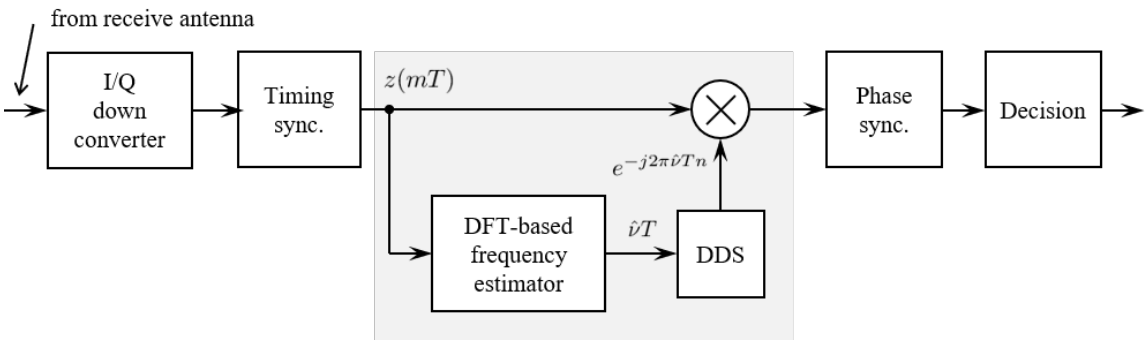

Figure 1: A fully synchronized 16-APSK detector emphasizing the frequency estimator.

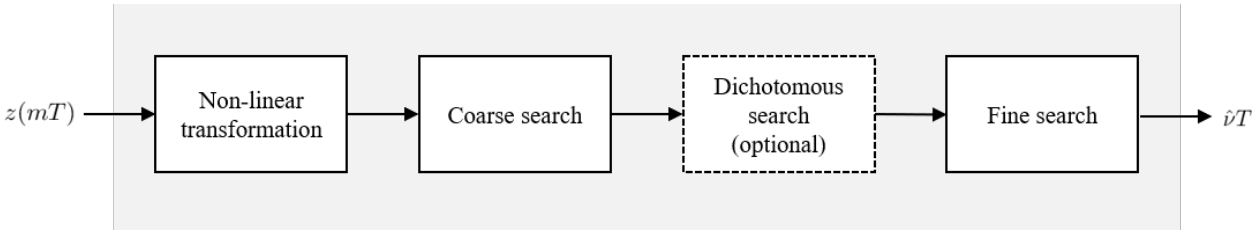

Figure 2: Detailed view of the DFT-based frequency estimator block in Figure 1.

signals. First, a non-linear transformation is applied to the matched filter outputs. Then the estimation process consists of two steps: the "coarse search" and the "fine search." The coarse search produces a rough frequency estimate by finding the absolute maximum of the periodogram of the matched filter outputs. The fine search then refines the accuracy of this frequency estimate. An optional "dichotomous search" may be inserted between the coarse and fine searches to further improve the frequency estimate. This refined frequency estimate is then used to derotate the received symbols. The process of phase synchronization and symbol decisions is outlined in [4]. The bit error rate (BER) of various frequency estimation methods is then analyzed, allowing for comparison of these methods.

CHANNEL MODEL

For our analysis, we simulated the transmission of L_ν 16-APSK symbols over an AWGN channel. The starting point is the matched filter output

$$z(mT) = c_m e^{j(2\pi\nu Tm+\theta)} + n_1(mT), \quad m = 0, \ldots, L_\nu - 1 \tag{1}$$

where c_m represents the m-th complex-valued symbol from the 16-APSK constellation shown in Figure 3, T is the symbol time, νT is a constant, but unknown, frequency offset with units cycles/second, θ is a constant phase offset, and $n_1(mT)$ is AWGN with variance σ^2. Frequency estimation requires removal of the phase shifts due to the 16-APSK symbols. This is accomplished by the nonlinear transformation

$$z'(mT) = F\left[\rho(m)\right] e^{j12\phi(m)} \tag{2}$$

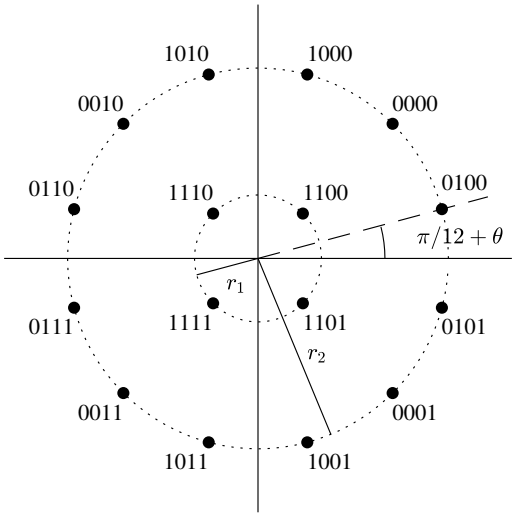

Figure 3: 16-APSK constellation

where

$$\begin{aligned} \rho(m) &= |z(mT)| \\ \phi(m) &= \arg\{z(mT)\} \\ F[x] &= x^k \end{aligned} \tag{3}$$

and k is an integer. We use $k = 2$ throughout this paper in order to account for the amplitude modulation of these signals. After this transformation, the frequency offset νT may then be estimated. This is accomplished by estimating

$$\hat{\nu}T = \underset{\nu T}{\operatorname{argmax}}\{|\sum_{m=0}^{L_\nu - 1} z'(mT)e^{-j2\pi\nu T m}|^2\} \tag{4}$$

where the expression to be maximized is the periodogram of the transformed signal. This estimation consists of the aforementioned coarse search followed by any of several fine searches.

COARSE SEARCH

The coarse search provides a frequency estimate as follows. The periodogram of the matched filter outputs is computed by taking the magnitude squared the signal's DFT. When the number of samples is a power of 2, the DFT can be calculated using highly-efficient FFT algorithms. In this paper, we use a length-$2L_\nu$ FFT, where L_ν is the number of received symbols. The argument that produces the maximum value of the periodogram is denoted $\hat{\omega}_M$. The frequency offset estimate $\hat{\nu}T$ is then calculated using the formula

$$\hat{\nu}T = \frac{1}{12}\frac{\hat{\omega}_M}{2\pi}. \tag{5}$$

This provides us with a "coarse estimate." This estimate is restricted to discrete values and may not provide a sufficiently accurate estimate to properly decode the symbols across the entire data

block. A fine search must be performed to provide a more accurate estimate to compensate for the frequency quantization error.

FINE SEARCH

Various methods have been proposed to interpolate intermediate values between the samples provided by the coarse search. We have identified three such methods and have adapted them for use with the 16-APSK modulation scheme. These three methods are described below and are compared in the Simulation Results section of this paper. In all three formulas, the two points from the periodogram on either side of the coarse frequency estimate are used. Here, the value of the periodogram to the left of the maximum is denoted P_1, the maximum is denoted P_2, and the value to the right is P_3.

One interpolator uses the formula

$$\hat{\omega} = \hat{\omega}_M + \frac{\delta_\omega}{4} \frac{P_1 - P_3}{P_1 - 2P_2 + P_3} \tag{6}$$

to perform a parabolic interpolation of the three points [1, 2]. In this paper, we call this "Interpolator 1." An alternate interpolator uses the formula

$$\hat{\omega} = \hat{\omega}_M + \frac{\alpha}{2L_\nu} \frac{P_0}{P_2 - P_0} \tag{7}$$

where

$$\begin{aligned} P_0 &= \max\{P_1, P_3\} \\ \alpha &= \operatorname{sign}\{P_3 - P_1\} \end{aligned} \tag{8}$$

which we will refer to as "Interpolator 2." A third "Gaussian interpolator" with the formula

$$\hat{\omega} = \hat{\omega}_M + \frac{1}{2L_\nu} \frac{\log P_1 - \log P_3}{\log P_1 - 2\log P_2 + \log P_3} \tag{9}$$

can also improve the coarse frequency estimate. Regardless of the method chosen for interpolation, the final frequency estimate is obtained by calculating νT from Eq. 5 using the fine estimate $\hat{\omega}$ instead of the coarse estimate $\hat{\omega}_M$. An example of improved estimator error variance is shown in Figure 4. The coarse estimate can be significantly improved by implementing Interpolator 1 described by Eq. 6.

DICHOTOMOUS SEARCH

An intermediate "dichotomous search" may be used between the coarse and fine searches in order to further increase the accuracy of the frequency estimate. This dichotomous search begins with the values of P_1, P_2, and P_3 from the coarse search algorithm as described above. We first define $\delta f = \frac{1}{2L_\nu}$, the frequency spacing between each FFT sample. An iterative algorithm is then applied to the frequency estimate as follows.

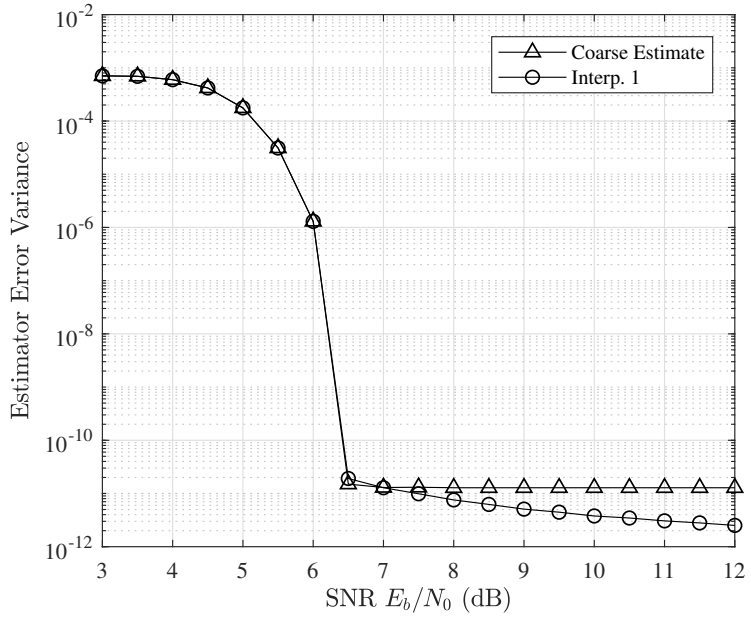

Figure 4: Variance of the coarse search with Interpolator 1 for $L_\nu = 1024$ and $\nu T = 0.012$.

1. First, δf is halved.
2. If $P_3 < P_1$, then P_3 is set to the value P_2 and the frequency estimate $\hat{f}$ is set to $\hat{f} - \delta f$. If $P_3 > P_1$, then P_1 is set to the value P_2 and the frequency estimate $\hat{f}$ is set to $\hat{f} + \delta f$.
3. The DTFT is evaluated at the new $\hat{f}$ using the formula $|\sum_{t=0}^{N-1} x_t e^{-j2\pi \hat{f} t}|^2$. This value becomes P_2.

These steps are repeated several times depending on channel properties such as SNR as outlined in [1]. The results of the dichotomous search are then passed on to the fine search for further refinement. Note that the effective length of the FFT has increased after the dichotomous search, so the interpolation formulas must be adapted according to the number of iterations applied during the dichotomous search.

SIMULATION RESULTS

Each of the above three interpolators have been simulated in MATLAB® with and without the use of a dichotomous search. In order to evaluate the performance of these frequency estimators, we compare the estimator error variances and BERs.

Each method demonstrates a high estimate error variance for low E_b/N_0 values as shown in the top plots of Figures 5, 6, and 7. As E_b/N_0 increases, the error variance generally decreases. Each estimator exhibits a precipitous drop in a "waterfall region," after which the variance decreases at a much slower rate. The point at which this slow decrease begins is referred to as the "corner value."

For $L_\nu = 512$ as shown in Figure 5, most of the estimators improve significantly after the waterfall region except Interpolator 2, which does not improve even at high SNRs. However, Interpolator 2 performs significantly better with $L_\nu = 1024$ as can be seen in the top plot of Figure 6.

The BER is a useful metric for quantifying the effectiveness of a given frequency offset estimator. This is illustrated in the bottom plots of Figures 5, 6, and 7 where we compare a given method's BER to the ideal AWGN BER. No method can achieve the ideal BER for small L_ν values, as shown in the bottom plot of Figure 5. At larger L_ν values, the BER of each interpolator approaches the ideal AWGN BER for sufficiently high SNRs. An example of a large L_ν is shown in Figure 7.

A comparison of various L_ν values for the dichotomous search paired with Interpolator 1 is given in Figure 8. The variance of the estimate error decreases and the BER approaches the ideal as L_ν increases. In addition, the corner value also migrates to lower E_b/N_0 values as L_ν increases. These are desirable traits for a frequency estimator as they allow effective estimation at lower SNRs. A longer FFT must be computed, however, which requires additional time and memory.

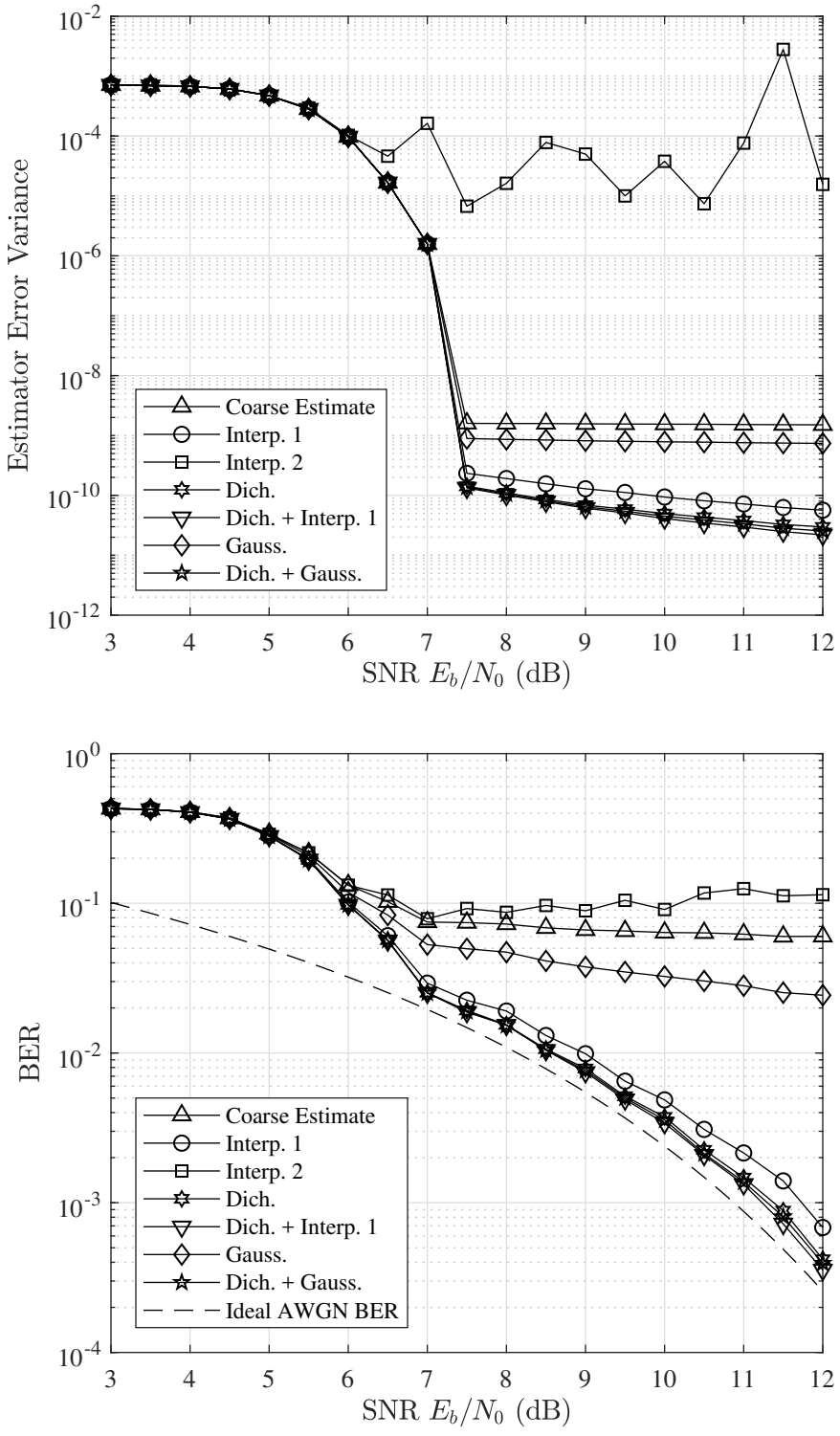

Figure 5: Simulation results for $L_\nu = 512$: (top) Estimator error variance; (bottom) BER.

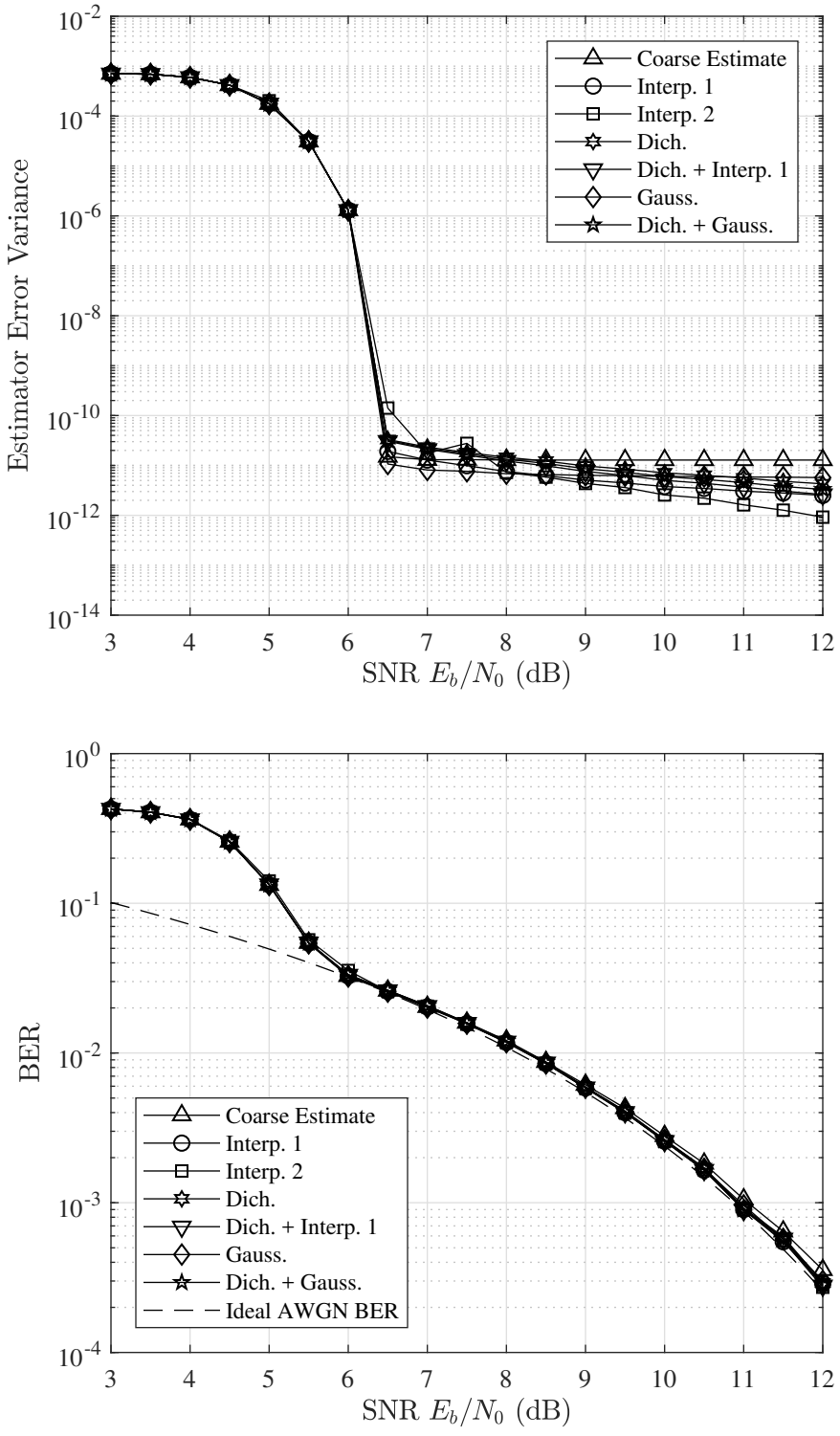

Figure 6: Simulation results for $L_\nu = 1024$: (top) Estimator error variance; (bottom) BER.

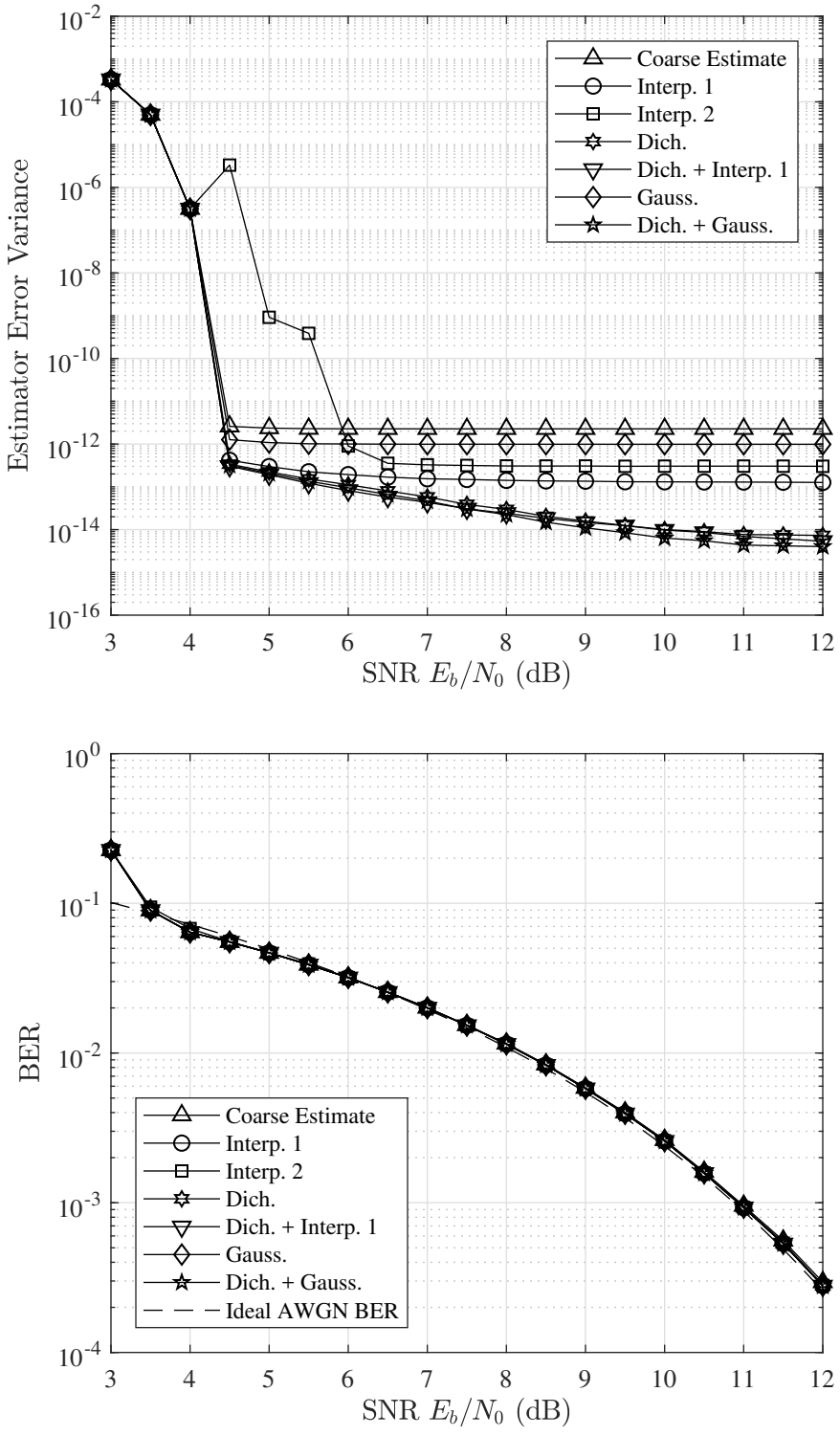

Figure 7: Simulation results for $L_\nu = 8192$: (top) Estimator error variance; (bottom) BER.

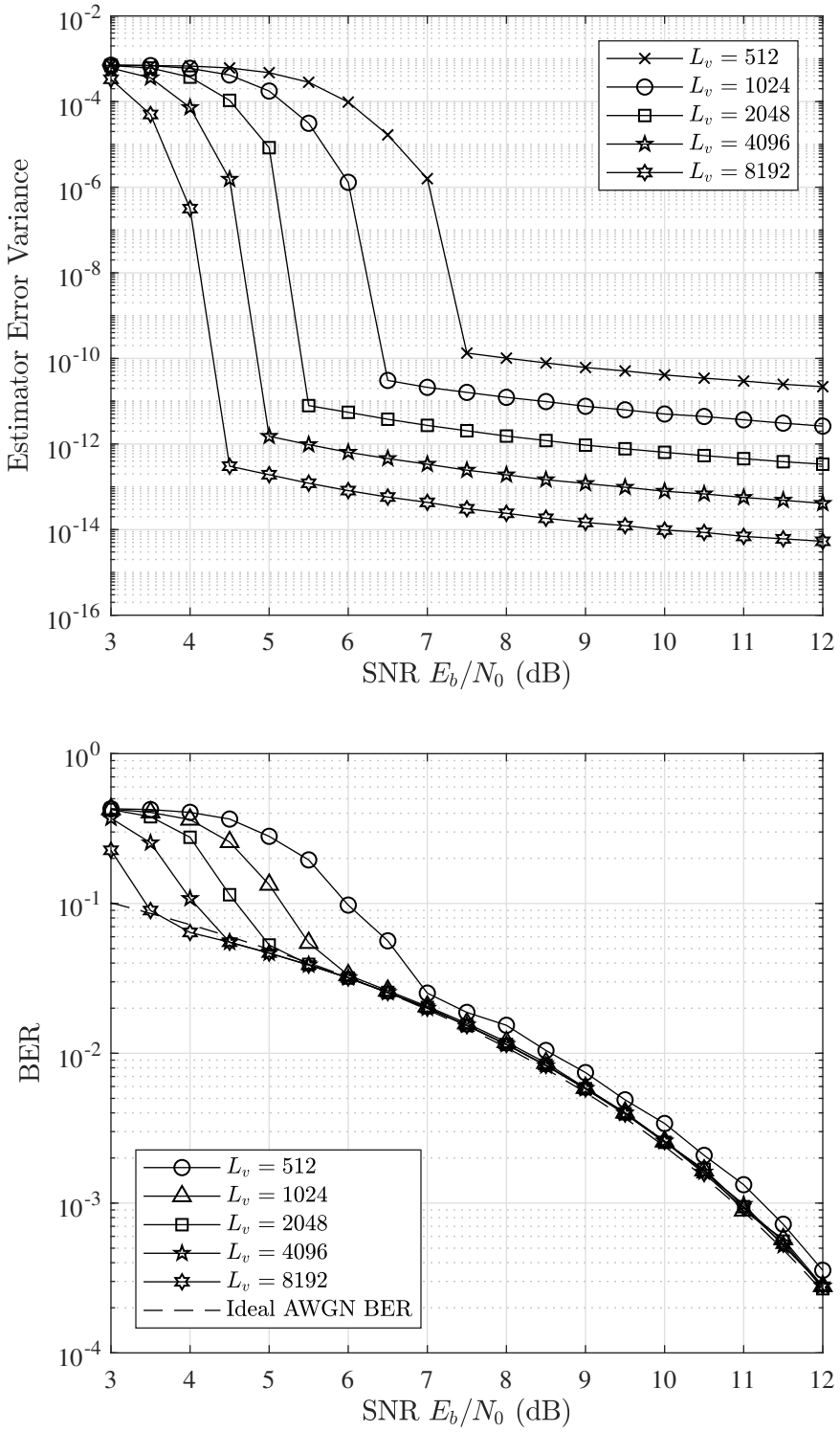

Figure 8: Simulation results for various values of L_ν using a dichotomous search and Interpolator 1: (top) Estimator error variance; (bottom) BER.

CONCLUSIONS

Here we demonstrate the viability of DFT-based frequency estimators adapted for 16-APSK. Such estimators provide sufficiently accurate estimates to allow for near ideal BERs. These methods consist of a coarse search, an optional dichotomous search, and a fine search. We compare estimator error variance and BER for various interpolation methods and DFT-lengths. For sufficiently long DFT-lengths, these estimation methods provide BERs close to ideal for AWGN channels.

REFERENCES

[1] Y. V. Zakharov, V. M. Baronkin, and T. C. Tozer, "DFT-based frequency estimators with narrow acquisition range," *IEE Proceedings - Communications*, vol. 148, pp. 1–7, Feb 2001.

[2] A. A. D'Amico, A. N. D'Andrea, and R. Regiannini, "Efficient non-data-aided carrier and clock recovery for satellite dvb at very low signal-to-noise ratios," *IEEE Journal on Selected Areas in Communications*, vol. 19, pp. 2320–2330, Dec 2001.

[3] E. Hosseini and E. Perrins, "Timing, carrier, and frame synchronization of burst-mode cpm," *IEEE Transactions on Communications*, vol. 61, pp. 5125–5138, December 2013.

[4] M. Rice, B. Redd, and X. Briceño, "On carrier frequency and phase synchronization for coded 16-APSK in aeronautical mobile telemetry," in *Proceedings of the International Telemetering Conference*, (Las Vegas, NV), 21-24 October 2019.